Microtexture and electromigration-induced drift in electroplated damascene Cu

doi: 10.1063/1.372258

Microtexture and electromigration-induced drift in electroplated damascene Cu

J. Proost[a)]
IMEC, Kapeldreef 75, B-3001 Leuven, Belgium and Department of Materials Science, K. U. Leuven, Belgium

T. Hirato and T. Furuhara
Department of Metallurgy, Kyoto University, Sakyo-ku, Kyoto 606-01, Japan

K. Maex[b)]
IMEC, Kapeldreef 75, B-3001 Leuven, Belgium

J.-P. Celis
Department of Materials Science, K. U. Leuven, Belgium

(Received 23 September 1999; accepted for publication 8 December 1999)

In this work, the electromigration (EM) performance of electroplated damascene Cu is investigated by drift experiments on Blech-type test structures in both polycrystalline and bamboo microstructures. For the first, microtexture data were obtained from electron backscatter diffraction as well. While both bonding areas and 10 μm wide lines were found to have a predominantly random grain orientation, the drift studies indicated the importance of strongly segregating impurities in controlling Cu grain-boundary EM. For the bamboo lines, the impact of different barrier layers has been investigated, comparing Ta, TaN, and TiN. Drift was shown to proceed in all cases at the metallic Cu barrier interface, but faster for the Ta as compared to the TaN and TiN barriers. Cu drift data were finally compared to available literature results and to our previous drift studies on Al(Cu). © *2000 American Institute of Physics.* [S0021-8979(00)05806-0]

I. INTRODUCTION

The efforts in replacing Al(Cu) by Cu as the interconnect material for sub-0.25-μm integrated circuits have resulted in the introduction of damascene-based metallizations, while electroplating has emerged as the preferred method for Cu deposition. In the damascene technology, instead of reactive ion etching (RIE) the interconnect from a continuous metallic film, prepatterned structures in the dielectric are filled with metal. The excess metal is then removed by chemical-mechanical polishing (CMP), leaving the interconnect embedded in the desired wiring pattern. The use of electroplating has brougth about some additional challenges related to the microstructural stability of Cu after deposition in terms of grain size and microtexture due to its room temperature recrystallization, generally known as Cu self-annealing.[1,2]

Two main factors have been driving the replacement of sputtered RIE Al(Cu) by electroplated damascene Cu for on-chip interconnects: lower resistivity and better electromigration (EM) performance. Although a relatively large amount of literature is available on Cu electromigration (reviewed in, e.g., Ref. 3), most experiments used classical lifetime testing on single-level RIE Cu structures. Only a few considered electroplated damascene Cu,[4] while no EM-induced drift experiments on damascene Cu have been reported. The basic difficulty related with EM lifetime tests on single-level structures ending in bonding reservoirs is that it measures EM-induced failure, rather than EM-induced mass transport. EM failure is generally caused by a complex series of physical and statistical processes, while EM-induced drift is captured more straightforwardly by the Nernst–Einstein relation

$$v_e = (eZ^*\rho j)\cdot \frac{D_{0,\mathrm{eff}}}{kT}\exp\left(-\frac{Q}{kT}\right) \tag{1}$$

with v_e the electromigration drift velocity, eZ^* the effective charge, ρ the resistivity, j the current density, Q the activation energy for mass transport, and kT having its usual meaning. $D_{0,\mathrm{eff}}$ is the effective preexponential factor of the diffusion coefficient, in the case of grain-boundary (GB) diffusion denoted as $D_0\delta/d, \delta$ being the effective GB width for mass transport and d the average grain size. In order to determine the drift velocity experimentally, a special method and test structure was developed by Blech and Kinsborn.[5] It is based on the direct observation of mass transport in a stripe of a relatively fast migrating metal (like pure Cu) deposited on top of a slow moving base conductor (like the barrier materials TiN, Ta, or TaN). The essential feature of a Blech structure is that it consists of an isolated block, clearly separated from the bonding region by the continuous barrier line. In that way, two additional flux divergence sites are created at the cathodic and anodic side, where current enters and leaves the block, respectively. The fact that for a pure metal, no voids or hillocks are observed inside the metal stripe during electromigration further indicates that these macrostructural flux divergences are dominant over the microstructural ones (such as triple points), the latter controlling EM failure in

a)Electronic mail: proost@deas.harvard.edu
b)Also at Department of Electronic Engineering, K. U. Leuven, Belgium.

classical lifetime structures. Therefore, by fixing the nature and location of the failure-controlling flux divergence sites, the complex series of physical and statistical processes encountered in lifetime testing reduces to the one controlling mass transport. The latter can typically also be studied under less severe accelerating conditions as compared to lifetime testing, where the failure time includes contributions from void nucleation and linkage towards an electrically detectable open circuit. Moreover, Blech structures also reflect more realistically the EM performance of interconnects in real circuitry, where similar macrostructural flux divergences are present at contacts or vias.

In previous work, we used drift experiments to characterize the EM performance of Al(Cu) in RIE and damascene Al(Cu), both for polycrystalline[6] and bamboo[7] microstructures. It is the aim of the present work to study the EM performance of electroplated damascene Cu by similar drift experiments on Blech structures, both for polycrystalline and bamboo lines. For the first, microtexture data as obtained from electron backscatter diffraction (EBSD) will be presented as well, while for the bamboo lines, the impact of different barrier layers will be investigated. Drift data will finally be compared to available literature results for Cu and to our previous drift data for Al(Cu).

II. EXPERIMENT

As test material, we used 500 nm deep damascene structures which were reactively ion etched in an 800 nm thick plasma enhanced chemical vapor deposited (PECVD) SiO_2 dielectric, deposited on a 6 in. Si wafer. For this work, 0.4, 0.7, and 10 μm wide isolated trenches were considered. Three different Cu metallizations were prepared. For the first two, an 80 nm thick Cu seed layer was sputtered without vacuum break onto a 150 nm thick physical vapor deposited (PVD) barrier layer of TaN and Ta, respectively. For the third, a vacuum break was included between sputtering of the 80 nm Cu seed and 20/100 nm Ti/TiN barrier layer. In all cases, the trenches were then filled with 1 μm of Cu in a commercially available electroplating tool and the excess Cu and barrier layer removed by CMP. Cu processing for the Ti/TiN samples (from here on referred to as the TiN samples) was different from the Ta and TaN samples in that both a different Cu plating bath chemistry and post-CMP clean was used. It should therefore be kept in mind that the effect of changing the barrier material can only be separated out when comparing the Ta vs TaN samples, for which both the same Cu plating and Cu CMP chemistry was used. The delay time between plating and CMP was at least one month for all samples, which were then kept for more than five months at room temperature after CMP before microtexture analysis and EM testing. Self-annealing is therefore believed to be completed.[1] Focused ion beam (FIB) top-view micrographs are shown in Fig. 1 for the 10 μm wide damascene lines. From these top-view FIB images, the circumference of more than 130 grains was traced manually and then used as a template for digital image analysis. Similar monomodal grain size distributions were obtained for all three samples, with an overall mean grain diameter of $0.75 \pm 0.05\ \mu$m.

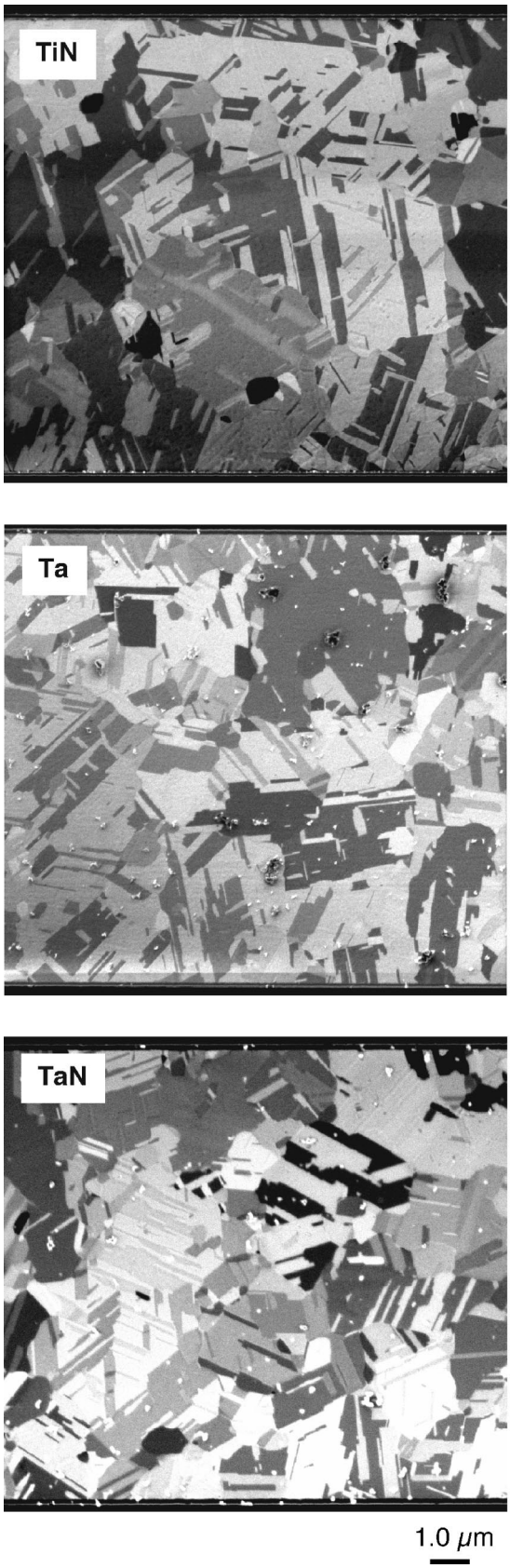

FIG. 1. op-view FIB micrographs on 10 μm wide electroplated damascene Cu for the TiN, Ta, and TaN samples.

From cross-sectional FIB micrographs, all samples showed a columnar grain structure. The microtexture of the electroplated damascene Cu lines was analyzed by EBSD, for which experimental details will be included in the next section.

To study EM-induced drift, additional processing was done to define Blech-type test structures. They consisted of one 100 ± 2 μm long Cu block, which was separated from the bonding region by the barrier base conductor. To process them, a second resist pattern was defined perpendicularly to the original damascene lines and used as a mask for wet chemically removing the uncovered part of the Cu selectively from the continuous barrier line. These Blech structures were then passivated with a 100 nm PECVD SiN_x. Before the actual EM testing, the test chips experienced some additional, though modest heat treatments, during and after packaging. The cure cycle for the polyimide, used to attach the die into the package cavity, was a sequence of 10 min at 150 °C and 10 min at 250 °C. In the EM test system, the ceramic, seam-sealed packages were heated at 5 °C/min to the EM furnace temperature, which was varied between 170 and 230 °C. Intermediate isothermal anneals were systematically inserted during ramping at 50, 75, and 100 °C for 1 h in order to determine the degree of Joule heating from the temperature coefficient of resistance.[8] An additional 1 h stay at the EM test temperature before current stressing was used for thermal stabilization. The test current density was fixed at 1.0 MA/cm^2, while the corresponding input current was accurately determined by considering the effective electrical cross section.[9] All drift experiments were performed in a DESTIN EM system with a specified temperature and current stability of 0.01 °C and 250 ppm, respectively.

III. RESULTS

A. Texture analysis by EBSD

For the EBSD analysis, a W-filament Hitachi HVE-3000 scanning electron microscope (SEM) was used, equipped with orientation imaging microscopy (OIM) from TSL, Inc.[10] To facilitate the EBSD measurements, only samples without the SiN_x passivation layer were investigated. Since no clear Kikuchi patterns could be obtained on the as-polished Cu samples, they were given an additional Ar ion milling. A SEM acceleration voltage of 23 kV was used and the sample surface was inclined 20° relative to the incident electron beam. Only EBSD data for 10 μm wide isolated damascene lines will be reported here. These will be compared to results for 100×100 μm^2 bonding areas for the Ta, TaN, and TiN samples. A hexagonal grid was used for scanning, with a frame averaging time of 0.8 s and a scan area of 50×20 μm^2 (bonding areas) and 100×10 μm^2 (10 μm line), respectively. For each condition, two scans were performed so that after omitting data points with a confidence index (CI) below 0.1, the total number of measurement points per condition was at least 20000.

1. Grain size data

Table I shows the average grain diameters as derived from the EBSD data. The angle defining contiguous grains was set to 5° and at least two measurement points were needed to define a grain. A distinction was made as well whether or not twins were considered as individual grains. In the first case (Table Ia), the average grain size is obviously smaller. In all cases, the grain size was found to be independent of the barrier layer. However, when comparing the bonding areas and the 10 μm line, a smaller grain size was consistently found for the latter, indicating that even for relatively wide 10 μm lines, grain growth in recessed damascene structures is geometrically restricted. Also striking is the fact that, when comparing the impact of not considering twins as individual grains (Table Ia vs Ib), the increase is relatively more pronounced for the bonding regions than for the 10 μm lines (factor 1.32 vs 1.19). This may be indicative for a higher twin boundary fraction in the bonding areas, as will be discussed later. Finally, the grain diameters as derived from plan-view FIB micrographs on isolated 10 μm lines statistically equal the ones calculated from the EBSD data.

TABLE I. Mean grain diameter (μm), as derived from EBSD and compared to the one obtained from FIB microscopy. Unlike the table on top (a), the table on the bottom (b) does not consider twins as individual grains. The angle defining contiguous grains was 5°.

Barrier	Bond area (EBSD)	10 μm line (EBSD)	10 μm line (FIB)
(a) Ta	1.01 ± 0.13	0.82 ± 0.08	0.70
TaN	0.95 ± 0.18	0.87 ± 0.01	0.76
TiN	1.15 ± 0.25	0.83 ± 0.13	0.80
overall mean Ta–TaN–TlN	1.04 ± 0.10	0.84 ± 0.03	0.75 ± 0.05
(b) Ta	1.35 ± 0.30	0.94 ± 0.10	
TaN	1.33 ± 0.45	1.14 ± 0.13	
TiN	1.44 ± 0.47	0.93 ± 0.11	
overall mean Ta–TaN–TiN	1.37 ± 0.06	1.00 ± 0.12	

2. Fiber volume fractions

The texture fractions for ⟨111⟩, ⟨110⟩, and ⟨100⟩ fibers are given in Table II for a tolerance angle of 10° around the sample surface normal. It can be seen that all samples were predominantly randomly oriented, with the texture analysis only accounting for about 30% of the texture fraction. This is

TABLE II. Fiber volume fractions (%) for ⟨111⟩, ⟨110⟩, and ⟨100⟩ obtained for a 10° tolerance angle from EBSD data.

	Bond area	10 μm line
Ta		
⟨111⟩	8.3 ± 1.5	13.0 ± 1.3
⟨110⟩	7.9 ± 4.1	7.4 ± 5.5
⟨100⟩	14.6 ± 3.8	15.2 ± 1.8
TaN		
⟨111⟩	8.8 ± 3.5	7.4 ± 0.1
⟨110⟩	6.7 ± 1.6	6.3 ± 1.0
⟨100⟩	14.6 ± 3.2	8.0 ± 1.6
TiN		
⟨111⟩	29.4 ± 12.4	12.8 ± 6.6
⟨110⟩	2.9 ± 0.9	7.0 ± 0.3
⟨100⟩	5.4 ± 2.8	6.0 ± 0.1

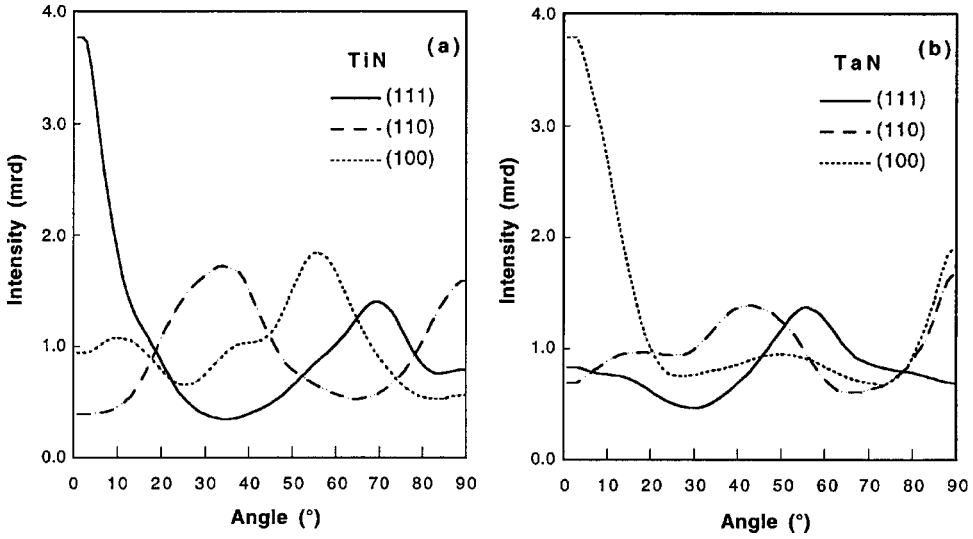

FIG. 2. Pole plots for a bonding area of the (a) TiN and (b) TaN sample, as calculated from the orientation distribution function using a 5° Gaussian half width for smoothing.

consistent with other reports,[11] in which texture weakening after self-annealing of an initially strong ⟨111⟩ fiber in electroplated Cu was attributed to the effect of multiple twinning in the early stages of the grain growth process.[12] However, while for a completely random texture, all components should occur in equal fractions, a slightly preferred ⟨100⟩ and ⟨111⟩ fraction was still observed in the Ta–TaN and TiN samples, respectively. Note that the fiber volume fractions for the Ta and TaN samples were very similar, which is attributed to their identical Cu processing. It is not clear why the ⟨100⟩ instead of the ⟨111⟩ fraction is the preferred one in the case of Ta–TaN. Assuming that all samples had a strong ⟨111⟩ fiber directly after plating, following other observations on electroplated Cu on a PVD Cu seed layer,[11] this may indicate that grain growth in the Ta–TaN samples has been more strongly driven by strain-energy minimization,[13] as opposed to grain boundary or surface energy minimization. It is speculated that this can be traced back to the difference in plating bath chemistry as compared to the TiN samples, especially to the amount of organic and inorganic additives.[14]

While it should be kept in mind that the grain orientation in all samples is predominantly random, the slightly preferred ⟨111⟩ fraction for the TiN and ⟨100⟩ fraction for the TaN samples is also illustrated in the pole plots of Fig. 2, which compares the results for a bonding area of the (a) TiN and (b) TiN sample. A pole plot represents an angular intensity distribution, normalized to units of multiples of a random distribution (mrd), of a specified pole relative to the sample normal. It was calculated from the orientation distribution function (ODF), using a 5° Gaussian half width. Figure 2 clearly shows the larger fraction of (111) and (100) planes oriented parallel to the sample surface for the TiN and TaN sample, respectively. Note that the other maxima refer to the same peaks as the fiber oriented peak. In the case of TaN, their position corresponds to the angle between (100) and (110) (45° and 90°), (111) (55°), and (100) (90°) planes, respectively, and for TiN between (111) and (110) (35° and 90°), (100) (55°), and (111) (70°) planes, respectively.

3. Grain-boundary structure

While the previous section highlighted aspects of macrotexture, more interesting with respect to EM-induced drift is the correlation with microtexture in terms of misorientation angle distribution and coincidence site lattice (CSL) fractions. Figure 3 plots the grain-boundary fractions as a function of misorientation angle for the 10 μm lines with Ta, TaN, and TiN barriers, respectively. Estimations for a randomly textured material are included as well.[15] Compared to the random distribution, misorientation distributions are only slightly shifted. Similar distributions were obtained for all

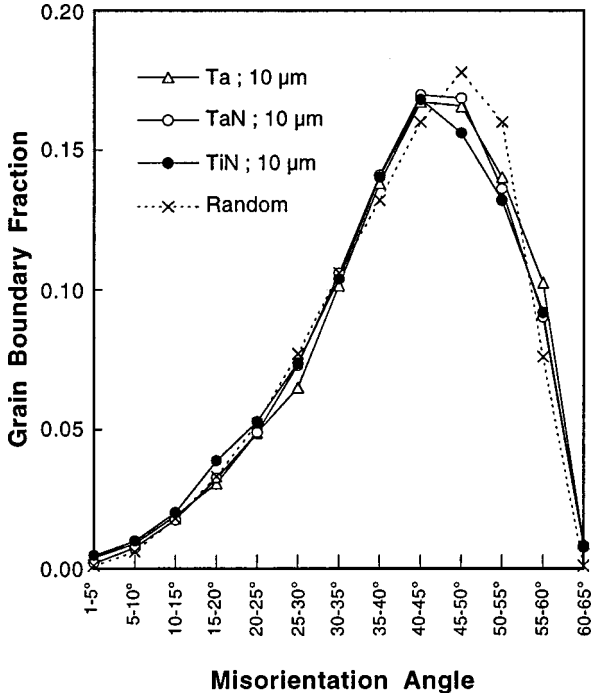

FIG. 3. Number fraction of grain boundaries as a function of misorientation angle for the 10 μm wide Ta, TaN, and TiN samples. The number fraction of boundaries in a randomly textured material (see Ref. 15) is given as a reference.

TABLE III. CSL fractions (%) for Σ3 and Σ5-29, respectively, obtained from EBSD data using Brandon's criteria[a] and considering a minimum boundary angle of 1°.

	Σ3		Σ5-29	
	Bond area	10 μm line	Bond area	10 μm line
Ta	0.31±0.02	0.26±0.02	0.071±0.005	0.068±0.019
TaN	0.32±0.03	0.30±0.05	0.076±0.009	0.086±0.001
TiN	0.25±0.04	0.18±0.02	0.066±0.018	0.068±0.019

[a]See Ref. 16.

samples, both when comparing the different barrier layers (Ta, TaN, TiN) and the effect of geometry (bonding areas versus 10 μm lines). More interesting are the CSL fractions, which were identified for a minimum boundary angle of 1° and using Brandon's criteria,[16] i.e., the CSL tolerance angle being $15°/\Sigma^{0.5}$. In all cases, a large fraction of Σ3 boundaries was observed, characteristic for twin boundaries. Table III gives the exact number fractions separately for Σ3 and Σ5–Σ29. For the latter, a variance analysis demonstrated all six conditions to result in statistically equal fractions (confidence level $\alpha=10\%$), with an overall mean of 0.073 ±0.007. For Σ3, however, distinct fractions were obtained, reflecting a corresponding difference in twinning probability. First, the Ta and TaN samples again gave similar results (*t* test, $\alpha=10\%$), both on the bonding areas and on the 10 μm lines. Therefore, both samples were averaged, with a mean Σ3 fraction of 0.32±0.01 for the bonding areas and 0.28 ±0.03 for the 10 μm lines. Second, when comparing the fractions between the bonding areas and the 10 μm lines, a higher twinning probability is anticipated for the bonding areas, both for the TiN and the Ta–TaN samples. A similar conclusion was already suggested from the grain size data in Table I, comparing values with/without considering twins as individual grains. However, a statistical analysis fails to find this difference significant (*t* test, $\alpha=10\%$). It may still be interesting to further investigate the effect of decreasing linewidth into the sub-micron region on twinning probability. Finally, contrary to the geometrical effect, the difference in Table III between the TiN and Ta–TaN samples was found to be significant, indicative for a lower twinning fraction in the TiN samples.

B. Electromigration performance

For the quantification of the Cu drift velocity, which is directly related to the Cu diffusivity through Eq. (1), the drifted volume must be determined with time. Typically, this is done by a direct inspection with optical or electron microscopy. Inspection of metal stripes after current stress, however, is time consuming and may require additional sample preparation in the case of passivated structures. Moreover, no information is present on the time dependence of drift, unless a multiple amount of samples is tested with time. As an alternative, the drift velocity was derived from the rate of resistance change of the Blech structure. In the case of a constant drift rate, it can be expressed as[17]

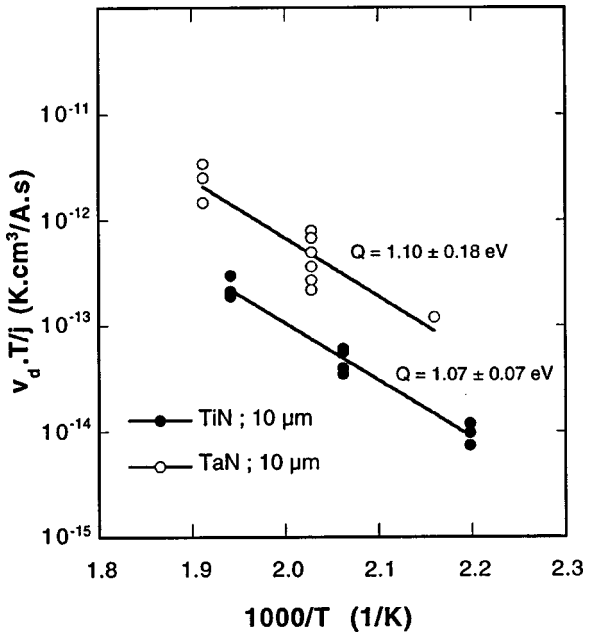

FIG. 4. Arrhenius plot for the drift velocity of electroplated damascene Cu as measured on the passivated polycrystalline 10 μm wide TiN and TaN samples.

$$v_d=\frac{w}{R_{s,b}}\frac{\partial R}{\partial t} \tag{2}$$

assuming a constant linewidth *w* and barrier sheet resistance $R_{s,b}$ and provided that the contribution of the Blech block to the total resistance can be neglected. Since for our structures, the initial stripe lengths that are covered and uncovered with Cu are equal and $R_{s,b}/R_{s,\mathrm{Cu}}>100$, Eq. (2) can indeed be used. The factor $R_{s,b}/w$ was calculated from the measured initial R^0_{tot} at the EM test temperature and test current, since $R_{s,b}/w\cong R^0_{\mathrm{tot}}/L^0_b$, L^0_b being the part of the Blech structure initially uncovered with Cu. No information about EM threshold could be derived from our experiments, so that v_d data could not be corrected for possible differences in critical length. These are especially expected when comparing the 0.4, 0.7, and 10 μm wide lines due to their different aspect ratio,[18] while the effect is expected to be less pronounced when comparing the different barrier layers or Cu microstructures.

1. Polycrystalline damascene Cu

For the 10 μm wide lines, drift experiments were performed on passivated TiN and TaN samples. The Arrhenius plot for the drift velocity v_d is shown in Fig. 4. The data points corresponding to the EM furnace temperatures of 170, 200, and 230 °C are shifted due to a difference in Joule heating. Both samples have statistically equal activation energies *Q*, averaging to 1.09±0.02 eV, but their absolute diffusivities differ by a factor 6.2±0.2, the lowest values measured for the TiN samples. Figure 5 shows optical microscope (OM) pictures after EM testing at a furnace temperature of 200 °C for 346 h. The inspected drift lengths for the TiN [Fig. 5(a)] and TaN [Fig. 5(b)] samples of 1.2 and 6.5 μm, respectively, agree fairly well with the ones based on the

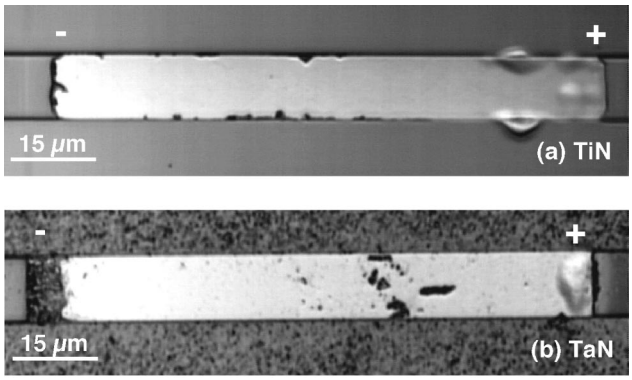

FIG. 5. Optical microscopy on a 10 μm wide (a) TiN and (b) TaN sample after EM at 1.0 MA/cm^2 for 346 h at a furnace temperature of 200 °C.

calculated drift velocities of 1.4 and 12.5 μm, respectively, assuming a constant drift rate during the 346 h of testing. A comparison with available literature data on Cu grain-boundary (GB) diffusion will be given later.

Although the texture analysis showed all samples to have a predominantly random texture, the 10 μm TiN lines had a statistically significant larger $\langle 111\rangle/\langle 100\rangle$ ratio as compared to the TaN ones (2.1 ± 0.5 vs 0.9 ± 0.2, cf. Table II). It may therefore be tempting to attribute the reduced drift rate of the TiN samples to a higher $\langle 111\rangle/\langle 100\rangle$ texture fraction, as proposed by Vaidya and Sinha.[19] However, this correlation, which is still a widely used argument to optimize texture for an improved EM performance, was based on EM-lifetime measurements, which generate statistical distributions of failure times in test structures ending in large bonding pads. As outlined previously, EM failure is in that case associated with open circuits developing at a microstructural flux divergence site. A stronger $\langle 111\rangle$ fiber texture will increase the EM lifetime because of the reduced degree of anisotropy in grain-boundary transport.[20] However, in our Blech structures, EM failure occurs as drift away from the cathode, the latter being a fixed physical flux divergence site, rather than as an open circuit at a microstructural flux divergence. Therefore, the role of grain-boundary structure in our case is restricted to determining the average diffusivity. In that respect, another argument commonly encountered in literature is that a preferred $\langle 111\rangle$ texture increases the EM performance by minimizing the amount of high-diffusivity high-angle grain boundaries.[4] In our case, this argument is to be rejected as well, since there was no difference in the misorientation angle distribution for the 10 μm wide TiN and TaN samples (cf. Fig. 3). A more plausible argument explaining the difference in drift rate will be presented in the discussion part and is based on recent observations[21] that the GB self-diffusivity of Cu is highly affected by strongly segregating impurities, even for Cu purities around 99,999%. The results of Fig. 4 therefore suggest that it is more likely the Cu plating bath chemistry, which was very different for the TiN and TaN samples, and the accompanying impurity level which has a strong impact on the EM performance of polycrystalline damascene Cu.

2. Bamboo damascene Cu

Drift experiments on bamboo lines were performed on passivated TiN, TaN, and Ta samples, with a linewidth of 0.4 and 0.7 μm. To validate their grain structures to be denoted as bamboo type, the maximum polycrystalline cluster lengths were calculated using the software tool Cluster 2.0.[22] For a lognormal grain size distribution with a median grain size of 0.6 μm (taken as a reasonable estimation based on the measured mean value of 0.75 μm for the 10 μm wide lines in Table I), a maximum polycrystalline clusterlength of 14 μm is obtained for a 0.7 μm wide line. As a consequence, the critical length should exceed 14 μm at our test current density of 1.0 MA/cm^2. Although no measurement of EM threshold could be done here, we obtained in previous work[18] for unpassivated 3.0 μm wide damascene Al(Cu) a threshold value of 1770 ± 100 A/cm. This is believed to be a safe lower limit for the threshold value of the 0.7 μm wide passivated damascene Cu studied in this work, so that the grain structure of the 0.7 and hence also of the 0.4 μm wide Cu line can reasonably be taken as bamboo type.

The Arrhenius plot for their drift velocity v_d is shown in Fig. 6(a) ($w=0.4$ μm) and Fig. 6(b) ($w=0.7$ μm). Also the data for the 10 μm wide polycrystalline TiN lines from Fig.

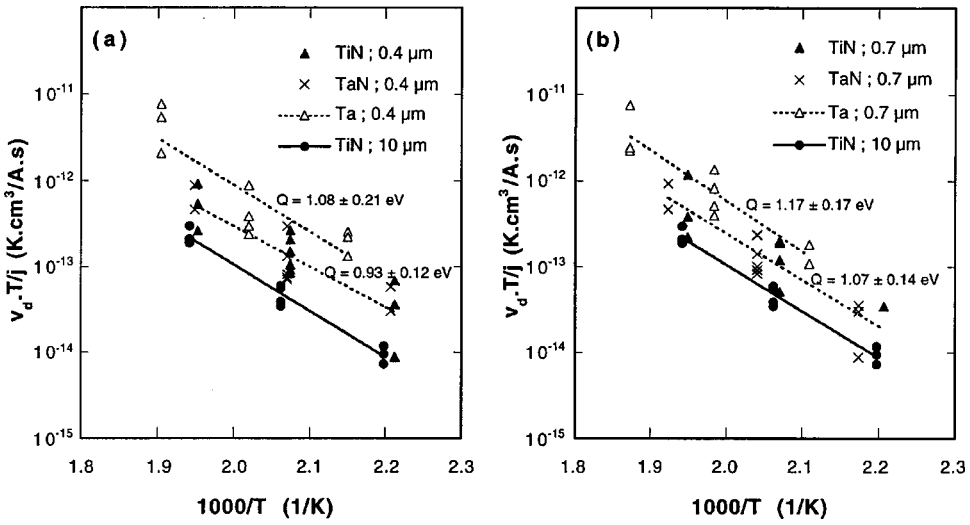

FIG. 6. Arrhenius plot for the drift velocity of electroplated damascene Cu as measured on (a) 0.4 μm and (b) 0.7 μm wide passivated bamboo TiN, TaN, and Ta samples. Also included are the data for the polycrystalline TiN samples. Drift rates in the bamboo TiN and TaN samples were found statistically equal and were combined in the Arrhenius fit.

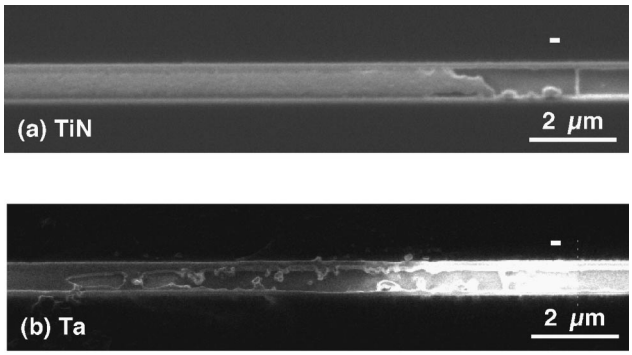

FIG. 7. FIB inspection of a 0.7 μm wide (a) TiN and (b) Ta sample after EM at 1.0 MA/cm^2 for 346 h at a furnace temperature of 200 °C. Micrographs were taken after *in situ* removal of the SiN_x passivation layer in the FIB. The Ta sample is tilted 20°.

4 are included as a reference. It is readily observed that in all cases, the bamboo lines drift at a higher rate than the best-performing, polycrystalline TiN samples. Contrary to the polycrystalline lines, the data for the TiN and TaN samples are now statistically equal, both for the 0.4 and 0.7 μm lines, although a large spread in drift velocity is recognized. Both data sets were therefore combined in the Arrhenius fit, resulting in an activation energy for the 0.4 and 0.7 μm TiN–TaN lines of 0.93 ± 0.12 and 1.07 ± 0.14 eV, respectively. The bamboo Ta samples showed a significantly higher drift rate than the TiN–TaN ones, the average difference being a factor 2.3 for both the 0.4 and 0.7 μm lines in the temperature range investigated. This difference will be sustained at the lower IC operating temperatures because of the equal activation energies. We will further use an overall mean Q value for the bamboo lines of 1.06 ± 0.10 eV. FIB micrographs of EM-induced drift are shown in Fig. 7 after 346 h of testing at a furnace temperature of 200 °C for a 0.7 μm wide TiN [Fig. 7(a)] and Ta [Fig. 7(b)] sample, respectively. The SiN_x passivation was first removed *in situ* in the FIB. The average drift velocities of Fig. 6(b) are 0.18 ± 0.09 and 0.98 ± 0.55 nm/min, respectively, predicting a total drift length after 346 h of 3.7 and 20.4 μm, respectively. These drift lengths are in reasonable agreement with the ones observed in Fig. 7 of 2.2 and 11.9 μm, respectively.

The fact that the bamboo TiN and TaN samples drift at similar rates suggests that their difference in Cu processing does not affect the EM performance of bamboo lines. The lower drift rate as compared to the Ta samples, which had a similar Cu processing as the TaN ones, rather indicates that it is the interface structure (e.g., coherency, defectivity) determined by the barrier material that controls the EM rate for electroplated Cu bamboo interconnects. As to the dominant diffusion path, lattice diffusion can reasonably be excluded based on its expected higher activation energy of 2.02 eV.[23] It would also have resulted in significantly lower drift velocities than the ones observed in Fig. 6. The different drift rate for the bamboo Ta vs the TiN–TaN samples rather suggests that it is the metallic interface with the barrier layer which provides the dominant diffusion path. There are two more arguments to identify the metallic interface and not the top interface with the SiN_x passivation as the dominant interfacial diffusion path. First, as discussed in our previous work on interfacial drift in bamboo Al(Cu),[7] the activation energies for GB- and interfacial diffusion are expected to be very similar, as the metallic interface provides a diffusion path similar to a grain boundary. This agrees with our data on Cu EM, the Q values for polycrystalline and bamboo lines being 1.09 ± 0.02 and 1.06 ± 0.10 eV, respectively. Second, if the top interface was the dominant diffusion path, no difference should be observed in the drift rates of the 0.4 and 0.7 μm wide lines. However, we do observe a higher drift velocity for the 0.4 μm lines, the difference with the 0.7 μm wide lines being a factor 1.4 for the TiN–TaN and 1.7 for the Ta samples. This difference will become even more close to the expected drift ratio of 0.7/0.4 after correcting for the expected higher EM threshold for the 0.4 wide lines.

IV. DISCUSSION

We will now critically compare our drift data on electroplated damascene Cu to available literature data on Cu EM and to our previously[6,7] reported drift data for RIE Al(Cu). Although several studies on Cu EM have been reported during the last decade, the attention here is focused on drift velocity rather than EM-lifetime tests. For Cu, drift velocity literature data were only found for RIE structures and none of them considered electroplated Cu. They are shown in Fig. 8, together with our current data on electroplated damascene Cu/TiN (bold lines) and our previous data on sputtered, RIE Al(Cu)/TiN (bold dashed lines). Details and references of the Cu literature data are given in Table IV.

Let us consider first the EM performance of polycrystalline Cu vs Al(Cu). When compiling literature data for pure Cu, a wide range of activation energies is reported, from 0.63 to 1.09 eV. The latter value was obtained for Cu evaporated onto TiN, while the first stems from a sputtered Ta/Cu/Ta stack. In between, an overall activation energy of 0.77 eV is obtained when extracting drift data scattered over three separate studies on Ta/Cu/Ta, including both evaporated and CVD Cu. Since GB diffusion is believed to be dominant, no effect of the cladding layers (TiN vs Ta) is to be expected in explaining the Q range. A similar range is observed from independent tracer and creep experiments on bulk Cu specimens (dashed lines i to iii in Fig. 8). Recently, the latter has been ascribed to a significant dependence of Cu GB self-diffusion on the Cu purity.[21] With sulpur being the main impurity element in that particular study, the activation energy for GB diffusion was found to increase from 0.75 eV for 99.9998% Cu to 0.88 eV for 99.999% Cu. Similar or even higher impurity levels can be expected for Cu thin film interconnects, depending on the deposition method. For CVD Cu, for instance, carbon and oxygen concentrations may exceed 0.1%,[27] while the highest purity can be expected for sputtered Cu. The difference between evaporated Cu/TiN and Ta/Cu/Ta still remains striking. A critical issue may be the RIE procedure, where for Cu/TiN, it was mentioned[29] that the TiN was patterned in a CF_4 plasma, using the pre-patterned Cu stripes as an etch mask. No such plasma exposure is inferred for the Ta covered Cu/Ta layers. In any case, it is believed from these observations that GB segregation of

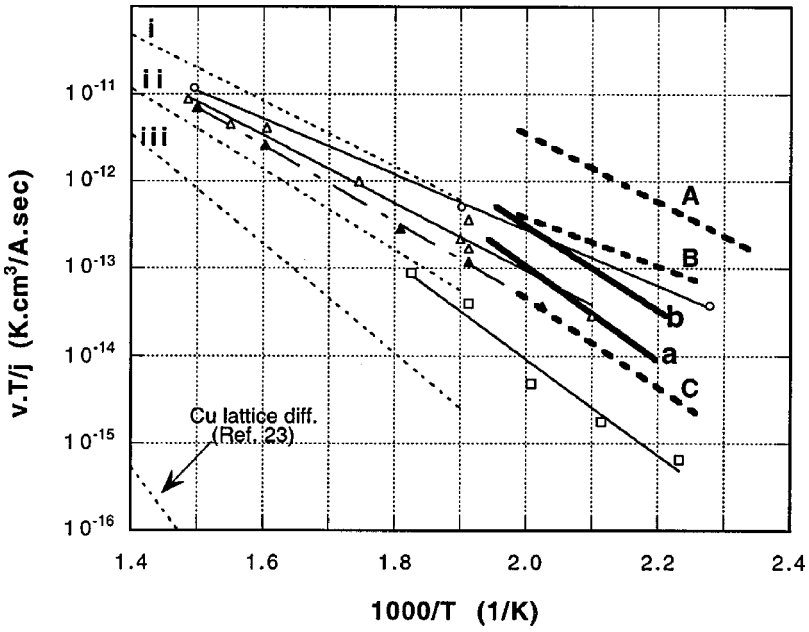

FIG. 8. Drift data obtained in this work (bold lines) on (a) polycrystalline and (b) bamboo electroplated damascene Cu/TiN, compared to both Cu-diffusivity data compiled from literature and Al drift data obtained in previous work (bold dashed lines) on RIE polycrystalline Al(Cu) (A), RTP-annealed RIE bamboo Al(Cu) (B) and as-patterned RIE bamboo Al(Cu) (C). More experimental details about the Cu literature data are given in Table IV. GB-diffusivity data from bulk studies were converted to drift velocities according to Eq. (1) for a grain size of 0.4 μm and with $q^*E = 83$ eV/cm (see Ref. 24). All bulk data were extrapolated to 250 °C, although in principle only Ref. 31 has taken data in that temperature range (cf. Table IV).

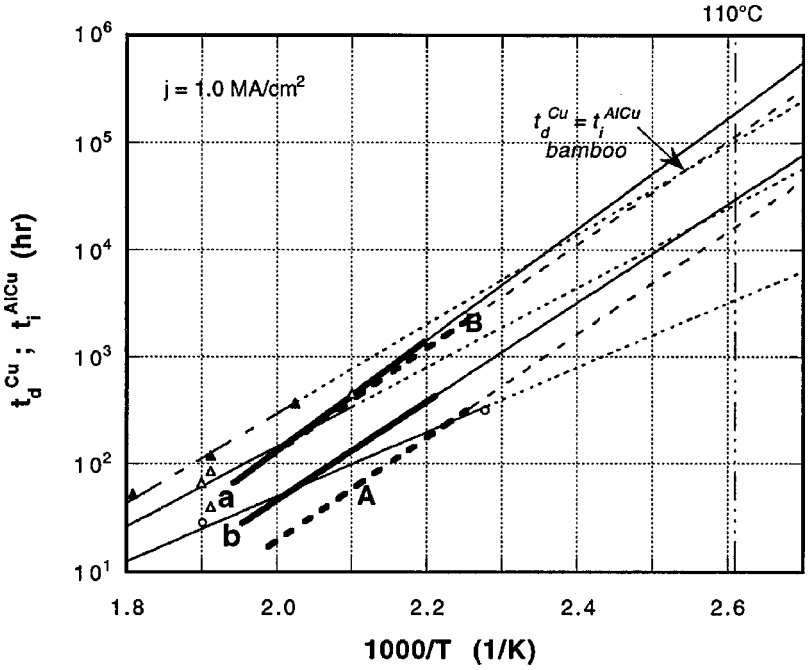

FIG. 9. Drift times for 1 μm Cu drift, extracted from Fig. 8 and compared at 1.0 MA/cm^2 to values for the incubation time in (A) polycrystalline and (B) bamboo Al(Cu).

TABLE IV. Some experimental details about the Cu drift and diffusivity literature data of Fig. 8.

Symbol Fig. 8	Ref.	T range (°C)	Q (eV)	Cu stack	Comments	$t/w/d_{50}$
○	25	166–396	0.63	Ta/Cu/Ta	sputtered	0.4/2.5/0.4 μm
△	26	250–400	0.77	Ta/Cu/Ta	evaporated	0.3/5.0/0.4
△	27	250–400	〃	〃	evap.+CVD	0.3/0.8-2/n.a.
△	28	200–394	〃	〃	evap.	0.3/2.0/0.4
□	29	175–275	1.09	Cu/TiN	evap.	0.5/11.5/1.35
▲	30	221–394	0.87	Ta/Cu/Ta	evap.	0.3/0.25/n.a
(i)	21	447–793	0.75	bulk Cu	tracer ^{64}Cu	3/8^{dia}/0.3 mm
(ii)	31	250–620	0.92	bulk Cu	tracer ^{67}Cu	3.2/9.5^{dia}/0.1
(iii)	32	539–819	1.24	bulk Cu	low T creep	wire/2.5^{dia}/0.04

t = thickness; w = width or diameter^{dia}; d_{50} = median grain size; n.a. = data not available

trace contaminations plays a vital role in Cu EM. When locating our data on electroplated damascene Cu, it can be noted that, while all Arrhenius curves from literature tend to intersect in one point at higher temperature, indicative of the so-called compensation effect,[33] our data seem to fall outside this regime. The relatively high activation energy of 1.07 eV still suggests a rather strong effect of segregating impurities. The latter may be attributed to the plating deposition process, not only due to the presence of organic additives, but also from the presence of sulphur in the acidified copper sulphate electrolyte. If sulphur is present in the electroplated Cu lines, it can indeed be expected to have a strong effect on Cu GB diffusivity because of its large segregation factor.[34] In this respect, the higher $\Sigma 3$ fraction observed in this work for the polycrystalline Cu/TaN lines will further enhance the anticipated effect of a different impurity level in explaining the increased drift rate as compared to the TiN lines. Although CSL boundaries are known to have a lower diffusivity compared to random high-angle boundaries for pure polycrystalline material, the situation may change significantly and even reverse in very diluted alloys.[35] This is generally ascribed to the fact that impurities have less tendency to segregate to CSL boundaries, making them ineffective in retarding CSL boundary diffusivity. A similar increase in drift velocity with increasing CSL fraction has been reported elsewhere[15] and is believed to confirm the major role of impurity segregation in controlling Cu GB electromigration in this work as well.

When comparing the Cu data in Fig. 8 to the one for sputtered, polycrystalline RIE Al(Cu) from our previous work,[6] at least one order of magnitude difference is observed at 200 °C. This difference will further increase at IC operating temperatures around 100 °C due to the higher activation energy associated with Cu GB diffusion. Hence, based on the drift velocity data alone, a significantly improved EM performance can indeed be expected for Cu, as is generally accepted in literature. However, we found that for Cu-alloyed Al, it is not the actual Al drift stage but the incubation time t_i, preceding Al drift, that becomes rate controlling at operating conditions.[6,18] The incubation time represents the time needed for the electron wind to deplete a region equal to the critical length free of Cu in the Al(Cu) stripe.[36] It is therefore controlled by both EM threshold and the kinetics of Cu depletion, the latter depending on the Al_2Cu precipitate morphology and distribution. We have shown that at operating conditions, it is the incubation time that controls the EM performance of Al(Cu), which in turn is dominated by the dissolution kinetics of Al_2Cu, with a characteristic activation energy of 1.05 ± 0.5 eV. Figure 9 compares our t_i values for Al(Cu) with 1 μm drift times (t_d), extracted from Fig. 8 for the RIE Ta/Cu/Ta stacks from literature and for our current drift data on damascene electroplated Cu. Compared to sputtered RIE Cu, Al(Cu) is seen to be superior at a device operating temperature of 110 °C, while a factor of 2 and 10 remains relative to RIE evaporated CVD Cu and our best-performing electroplated damascene Cu, respectively. The latter difference will further reduce when additionally extrapolating to use current, thanks to a higher current exponent for t_i ($n \cong -1.5$ from our work)[8] relative to t_d ($n = -1$ from the Nernst–Einstein relation). Obviously, these proportions will change by relaxing the Cu failure drift length above 1 μm. On the other hand, also the t_i values can be increased, as was illustrated in the Al(Cu) work by further optimizing the metallurgy of Al_2Cu precipitation, by an additional passivation layer or by using damascene instead of RIE Al(Cu).[6] Our results therefore indicate that for polycrystalline Cu vs Al(Cu), the claim of EM-superiority Cu is not justified. It would only be achieved through the presence of specially selected, strongly segregating impurities, which should drastically affect the Cu GB diffusivity but at the same time have a sufficiently low concentration in the bulk to maintain good electrical conductivity. A more controllable way would be to find a Cu-based alloy system, having the same sequential drift mechanism as was observed for Al(Cu). This can, for instance, be processed by alloying the PVD Cu seed layer and would allow to benefit also for Cu from a similar incubation component in the total drift time. A promising alloying element in this respect may be Sn,[26] besides Zr[28] and Ti.[37]

As to bamboo Cu interconnects, only one drift study was found in literature, reporting on a 0.25 μm wide evaporated RIE Ta/Cu/Ta stack.[30] Besides GB EM, also lattice EM can be excluded to have contributed to these data, based on the data of Maier[23] in Fig. 8. Therefore, the metallic Cu/Ta interface is believed to be the dominant diffusion path, with an interfacial diffusivity closely approaching the one for GB mass transport in evaporated Cu. An even higher drift velocity was measured for our 0.4 μm wide electroplated damascene Cu/TiN samples. Further research should clarify the origin of the relatively large drift velocities observed in bamboo Cu. It can be speculated that the sensitivity of Cu for twinning may be an important factor in increasing the interfacial defectivity and diffusivity. This may also explain the increased drift for electroplated bamboo lines, since they are more subject to twinning as compared to evaporated films during room temperature recrystallization.

Comparing the EM performance of bamboo Cu with our previous results on bamboo RIE Al(Cu)/TiN[7] reveals that the claim of Cu superiority is also not justified for bamboo interconnects. We will concentrate here on the best-performing literature data on RIE bamboo Cu/Ta stacks, which were superior to our nonoptimized EM performance of electroplated damascene Cu/TiN. For RIE bamboo Al(Cu)/TiN, both lattice and interface electromigration were found to be active, depending on the Cu distribution in the line.[7] In the case where lattice EM is dominant for Al(Cu) (bold dashed curve C in Fig. 8), the drift velocity becomes similar to the one for RIE Cu/Ta around 235 °C. In the case where interfacial EM is operative in Al(Cu) (bold dashed curve B), the drift velocity of pure Cu is found to be an order of magnitude lower at 200 °C. However, similarly as in polycrystalline interconnects, the incubation time for Al(Cu) is again able to make its EM performance superior to the one for pure Cu at use conditions, as illustrated in Fig. 9. The latter figure also allows to disagree with other recent claims of superiority of bamboo Cu vs Al(Cu), outlined in Refs. 38 and 39. Despite the lack of experimental details, at least two factors may have generated their misleading conclusions. First, tests were performed at highly accelerated conditions, up to 295 °C.

Figure 9 shows that in that case, the contribution of the incubation time to the total EM lifetime in Al(Cu) is only minor. Second, Cu results were compared to RIE bamboo Al(Cu)/$TiAl_3$ stacks, for which the incubation time was shown in our previous work[7] to be an additional factor 5 lower than for Al(Cu)/TiN. The only way to effectively make the EM performance of bamboo Cu superior to Al(Cu) would again be by alloying. This would allow to benefit also for Cu from an incubation time, provided the alloying element remains retarding on the interfacial diffusivity. Moreover, if alloying would succeed in suppressing interfacial EM in bamboo Cu, the gain in (lattice) EM performance at use temperature would be more than ten orders of magnitude.

V. CONCLUSIONS

In this work, the EM performance of electroplated damascene Cu has been investigated by drift experiments on passivated Blech-type test structures in both polycrystalline and bamboo microstructures. Samples with a Ta, TaN, and TiN barrier layer were studied, while the Ta and TaN samples received a different Cu processing from the TiN ones. For the 10 μm wide polycrystalline lines, drift in both the TiN and TaN samples was found to proceed with an activation energy of 1.09 ± 0.02 eV, but with a factor 6 slower in the TiN samples. Texture analysis by EBSD showed that for all lines, the $\langle 111 \rangle$, $\langle 110 \rangle$, and $\langle 100 \rangle$ fiber fractions only accounted for about 30% of the texture fraction, indicating a predominantly random grain orientation. Although the $\langle 111 \rangle / \langle 100 \rangle$ ratio was slightly higher for the 10 μm wide TiN as compared to the Ta and TaN lines, which both had similar fiber fractions, the reduced drift rate for the TiN samples was attributed to the difference in Cu plating chemistry and the anticipated difference in Cu purity, rather than to the slightly stronger (111) texture.

As to bamboo lines, the drift velocities derived for the Ta samples were consistently higher by a factor 2.3 than the ones with a TiN or TaN barrier, the latter two showing no statistical difference in drift rate. Drift in all bamboo lines showed similar activation energies, the overall mean of 1.06 ± 0.10 eV also being identical to the one characteristic for Cu GB electromigration. Drift in our bamboo lines was therefore believed to proceed by interfacial diffusion along the metallic interface with the Ta, TaN, and TiN barrier layer, providing a diffusion path similar to a grain boundary. Predominant diffusion along these metallic interfaces was also confirmed by the higher drift rate, about a factor 1.6, when going from 0.7 to 0.4 μm wide bamboo lines. The fact that the bamboo TiN and TaN samples drifted at similar rates suggested that their difference in Cu plating did not affect the EM performance. The slower rate as compared to the Ta samples, which had a similar Cu processing as the TaN ones, rather indicated that it is the interface structure, determined by the actual barrier material, that controls the EM rate for electroplated Cu bamboo interconnects. Drift in bamboo lines was also found to proceed faster as compared to the best-performing, polycrystalline TiN samples.

When comparing the Cu drift data from this work and other available literature to the EM-induced drift behavior of Al(Cu), the claim of EM superiority for Cu at IC operating conditions does not seem justified. This is caused by the fact that, although the drift velocities for Cu are significantly lower than for Al in Al(Cu), it is not the actual Al drift stage in Al(Cu), but the incubation period, preceding Al drift and dominated by the kinetics of Al_2Cu dissolution, that becomes rate controlling at use conditions.

ACKNOWLEDGMENTS

It is a pleasure to acknowledge S. Ogawa, Y. Awakura, and T. Maki for their interest in this work. One of the authors (J.P.) wishes to thank K. Murase, S. Morito, S. Zaefferer, and T. Shigetomi for their suggestions during the EBSD measurements, D. Chiaradia and I. Vervoort for their help during Cu processing and C. Drijbooms for FIB analysis. K.M. is a research director of the Fund for Scientific Research Flanders.

[1] C. Lingk and M. E. Gross, J. Appl. Phys. **84**, 5547 (1998).
[2] D. P. Field and M. M. Nowell, in *4th International Conference on Recrystallization and Related Phenomena*, Tsukuba, Japan, edited by T. Sakai and H. G. Suzuki (Japan Inst. of Metals, 1999), p. 851.
[3] J. R. Lloyd and J. J. Clement, Thin Solid Films **262**, 135 (1995).
[4] L. Vanasupa, Y.-C. Joo, P. R. Besser, and S. Pramanick, J. Appl. Phys. **85**, 2583 (1999).
[5] I. A. Blech and E. Kinsborn, Thin Solid Films **25**, 327 (1975).
[6] J. Proost, A. Witvrouw, J. D'Haen, P. Cosemans, and K. Maex, J. Appl. Phys. **87**, 86 (2000).
[7] J. Proost, K. Maex, and L. Delaey, J. Appl. Phys. **87**, 99 (2000).
[8] J. Proost, I. Samajdar, A. Witvrouw, and K. Maex, Mater. Res. Soc. Symp. Proc. **516**, 89 (1998).
[9] J. Proost, H. Li, T. Conard, W. Boullart, and K. Maex, J. Electrochem. Soc. **146**, 4230 (1999).
[10] TSL, Inc. OIM Software Version 2.5 User Manual, Draper, UT (1997).
[11] C. Lingk *et al.* MRS Proceeding on Advance Metallization Conference, 1999, p. 73.
[12] G. Gottstein, Acta Metall. **32**, 1117 (1984).
[13] J. M. E. Harper, C. Cabral, P. C. Andricacos, L. Gignac, I. C. Noyan, K. P. Rodbell, and C.-K. Hu, J. Appl. Phys. **86**, 2516 (1999).
[14] S. H. Brongersma, E. Richard, I. Vervoort, H. Bender, W. Vandervorst, S. Lagrange, G. Beyer, and K. Maex, J. Appl. Phys. **86**, 3642 (1999).
[15] J. Proost, I. Samajdar, B. Verlinden, P. Van Houtte, K. Maex, and L. Delaey, Scr. Metall. **39**, 1039 (1998).
[16] D. G. Brandon, Acta Metall. **14**, 1479 (1966).
[17] A. S. Oates, J. Appl. Phys. **70**, 5369 (1991).
[18] J. Proost, K. Maex, and L. Delaey, Appl. Phys. Lett. **73**, 2748 (1998).
[19] S. Vaidya and A. K. Sinha, Thin Solid Films **75**, 253 (1981).
[20] D. B. Knorr and K. P. Rodbell, J. Appl. Phys. **79**, 2409 (1996).
[21] T. Surholt and Chr. Herzig, Acta Mater. **45**, 3817 (1997).
[22] C. V. Thompson and W. Fayad, Cluster 2.0 (software), Dept. of Materials Science and Engineering, Massachusetts Institute of Technology, 1997.
[23] K. Maier, Phys. Status Solidi B **44**, 567 (1977).
[24] F. M. d'Heurle and A. Gangulee, Thin Solid Films **25**, 531 (1975).
[25] C.-K. Hu, M. B. Small, and P. S. Ho, Mater. Res. Soc. Symp. Proc. **260**, 730 (1992).
[26] K. L. Lee, C.-K. Hu, and K. N. Tu, J. Appl. Phys. **78**, 4428 (1995).
[27] C.-K. Hu, B. Luther, F. B. Kaufman, J. Hummel, C. Uzoh, and D. J. Pearson, Thin Solid Films **262**, 84 (1995).
[28] C.-K. Hu, K. Y. Lee, K. L. Lee, C. Cabral, E. G. Colgan, and C. Stanis, J. Electrochem. Soc. **143**, 1001 (1996).
[29] R. Frankovic and G. H. Bernstein, IEEE Trans. Electron Devices **43**, 2233 (1996).
[30] C.-K. Hu, K. Y. Lee, L. Gignac, and R. Carruthers, Proceedings of the

Fourth International Workshop on Stress Induced Phenomena in Metallization, 1998, p. 113.
[31] D. Gupta, Mater. Res. Soc. Symp. Proc. **337**, 209 (1994).
[32] B. Burton and G. W. Greenwood, Met. Sci. **4**, 215 (1970).
[33] E. Glickman and M. Natan, J. Appl. Phys. **80**, 3782 (1996).
[34] F. Moya and G. E. Moya-Gontier, Scr. Metall. **9**, 307 (1975).
[35] K. T. Aust and J. W. Rutter, Trans. AIME **215**, 120 (1959); **215**, 820 (1959).
[36] C.-K. Hu, P. S. Ho, and M. B. Small, J. Appl. Phys. **72**, 291 (1992).
[37] K. Hoshino, H. Yagi, and H. Tsuchikawa, IEEE Proc. VMIC, 357 (1990).
[38] S. Venkatesan *et al.*, IEEE Proc. IEDM, 769 (1997).
[39] D. Edelstein *et al.*, IEEE Proc. IEDM, 773 (1997).